Measurement of ion cascade energies through resolution degradation of alpha particle microcalorimeters

Robert D. Horansky,[1,a)] Gregory M. Stiehl,[1] James A. Beall,[1] Kent D. Irwin,[1] Alexander A. Plionis,[2] Michael W. Rabin,[2] and Joel N. Ullom[1]
[1]*National Institute of Standards and Technology, 325 Broadway MS 817.03, Boulder, Colorado, USA*
[2]*Los Alamos National Laboratory, Los Alamos, New Mexico 87545, USA*

(Received 21 September 2009; accepted 7 January 2010; published online 25 February 2010)

Atomic cascades caused by ions impinging on bulk materials have remained of interest to the scientific community since their discovery by Goldstein in 1902. While considerable effort has been spent describing and, more recently, simulating these cascades, tools that can study individual events are lacking and several aspects of cascade behavior remain poorly known. These aspects include the material energies that determine cascade magnitude and the variation between cascades produced by monoenergetic ions. We have recently developed an alpha particle detector with a thermodynamic resolution near 100 eV full-width-at-half-maximum (FWHM) and an achieved resolution of 1.06 keV FWHM for 5.3 MeV particles. The detector relies on the absorption of particles by a bulk material and a thermal change in a superconducting thermometer. The achieved resolution of this detector provides the highest resolving power of any energy dispersive technique and a factor of 8 improvement over semiconductor detectors. The exquisite resolution can be directly applied to improved measurements of fundamental nuclear decays and nuclear forensics. In addition, we propose that the discrepancy between the thermodynamic and achieved resolution is due to fluctuations in lattice damage caused by ion-induced cascades in the absorber. Hence, this new detector is capable of measuring the kinetic energy converted to lattice damage in individual atomic cascades. This capability allows new measurements of cascade dynamics; for example, we find that the ubiquitous modeling program, SRIM, significantly underestimates the lattice damage caused in bulk tin by 5.3 MeV alpha particles. © *2010 American Institute of Physics*. [doi:10.1063/1.3309279]

I. INTRODUCTION

Interest in the interaction of ions with matter spans many fields including fundamental measurements of stopping powers,[1] cascade dynamics,[2] ion implantation,[3] and radiation detection.[4] The highest resolution ion detectors available to this diverse population of researchers are based on charge collection in semiconductors. These detectors are fundamentally limited by Fano statistics to 8–10 keV full-width-at-half-maximum (FWHM) resolution for 5 MeV alpha particles.[5] By using a very different sensing mechanism, namely calorimetry with a superconductor as the thermometer, we are able to achieve resolutions as good as 1.06 ± 0.04 keV FWHM for 5.3 MeV alpha particles, which is the highest resolving power of any energy dispersive technique to date.[6]

The resolution improvement derives from using the reduced thermodynamic noise at typical operating temperatures of 0.1 K. This technique has been used to achieve precise energy measurements of individual optical,[7] x-ray,[8] and gamma-ray photons,[9,10] in addition to biomolecules[11] and now, alpha particles.[6] Because the characteristic linear dimension of these sensors ranges from tens of microns to approximately 1 mm, they are known as microcalorimeters. With a resolution near 1 keV FWHM, several applications for ultrahigh resolution alpha spectrometry become feasible. In recent work, we made the first direct determination of the branching ratio to the ground state in the decay of ^{209}Po.[6] In nuclear security, alpha particle spectrometry is a vital tool for characterizing trace quantities of nuclear material. It has recently been emphasized by the International Atomic Energy Agency[12] and numerous scientific panels[13,14] that the development of new technology for nuclear forensic applications is of utmost concern. The resolution limits of Si-based alpha detectors necessitates time consuming chemical separation of actinides before alpha measurement. With a near-ten-fold improvement in resolving power, mixed actinide samples can be measured directly, reducing analysis times from weeks to days. A prototype microcalorimeter spectrometer is currently being assembled for rapid analysis of trace samples.[15]

Although the 1 keV resolution achieved by the microcalorimeter is already sufficient for applications, the resolution predicted from the thermodynamics of the detector and from measurements of photons and internal noise is approximately 0.1 keV FWHM. A possible explanation can be found in the work of Andersen who assessed cryogenic bolometers for astronomical use. Andersen[16] predicted that fluctuations in atomic movement in the absorber due to the incident alpha particles would limit the resolution of cryogenic calorimeters to approximately 1 keV. In more recent work, Juillard[17] used the software package SRIM to predict 1 keV fluctuations in lattice damage for a Cu absorber. However, it is only now that other noise terms in a microcalorim-

[a)]Electronic mail: horansky@nist.gov.

 © 2010 American Institute of Physics

Downloaded 07 Sep 2010 to 132.163.130.218. Redistribution subject to AIP license or copyright; see http://jap.aip.org/about/rights_and_permissions

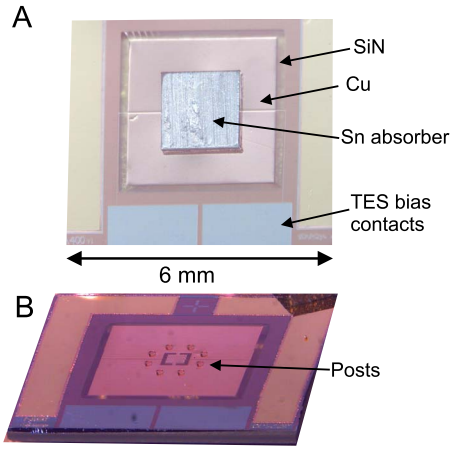

FIG. 1. (Color online) (a) Micrograph of the alpha particle detector with the Sn absorber covering the TES. The Cu thermalization layer and the SiN isolation are clearly seen. The pads for electrical contact by wire bonding are shown at the bottom and the edge is patterned with gold so that gold wire bonds provide more thermal sinking. (b) Micrograph of same chip before the absorber is glued to the photoimagable posts. The TES is the square film in the middle of the chip and is connected by two fingers to the surrounding Cu film.

eter have been sufficiently reduced that this fundamental limit can be probed.

In what follows, we first describe the microcalorimeter detector and the measurement setup. Next, we describe the thermodynamic resolution limit of the microcalorimeter and demonstrate the presence of a discrepancy between the fundamental and achieved resolutions of the device. Then, we review possible explanations for this discrepancy and calculate their magnitudes. Possible resolution degradation mechanisms are position dependence in the sensor response, temperature fluctuation in the cryostat, sputtering of atoms, secondary electron emission, phase dependent external noise, detector gain drift, and anomalous thermalization in the superconducting absorber. We show that these mechanisms are all minor, leaving lattice damage fluctuations as the sole remaining explanation for the achieved resolution. Finally, we show how measurements of the energy converted to lattice damage can be used to constrain the materials parameters that determine cascade dynamics: the Frenkel, binding, and displacement energies.

II. THE EXPERIMENTAL SETUP

Alpha particle microcalorimeters consist of three elements: an absorber to convert the alpha particle kinetic energy into thermal excitations, a thermometer to register the resultant temperature change, and a thermal weak link between these elements and a temperature bath so that the heat may be collected and then dissipated with a time constant appropriate to the needed count rate. The absorber is bulk, superconducting tin (Sn). The low heat capacity of a superconducting absorber provides an excellent signal-to-noise ratio, while allowing good collection area and stopping power.[9] The absorber is $1.7\times1.7\times0.25$ mm^3 and is shown in Fig. 1(a). The thermometer for our alpha detector is a transition-edge sensor (TES).[18] The TES is a superconducting thin-film bilayer of molybdenum and copper that is voltage-biased at its superconducting transition temperature of 140 mK, where a small change in temperature results in a large change in resistance. The TES is shown in Fig. 1(b) where the absorber has been removed. The absorber is attached to the TES chip by gluing on the top of eight posts made from a photoimagable epoxy. The posts can be seen in Fig. 1(b). The posts are 40 μm tall and 200 μm in diameter. The distributed epoxy posts allow large area absorbers to be supported. The posts are attached at the bottom to a copper thermalization layer on the TES chip whose dimensions are 3.2 mm $\times$3.2 mm$\times$0.5 μm. The Cu thermalization layer allows fine tuning of the detector heat capacity and allows mechanically stable attachment of the absorber without causing stress in the TES. The Cu layer attaches to the TES through two small Cu fingers. The whole detector is fabricated on a silicon chip $6.35\times6.35\times0.28$ mm^3 with an additional layer of silicon nitride 0.5 μm thick on top. The Si underneath the SiN at the center of the chip is removed by deep reactive ion etching so that the TES and Cu thermalizing layer are thermally isolated from the Si substrate. The Si is heat sunk to a copper mount that is maintained at 80 mK and is the heat bath.

The microcalorimeter detector works just as any calorimeter, by measuring energy deposited in a thermally isolated body. Alpha particles absorbed by the Sn create excitations through ionization and nuclear interactions. The excitations then scatter through various mechanisms to create phonons. The phonon energy thermalizes in the Sn, then travels through the posts to thermalize in the Cu and TES below. The TES measures the temperature change before the energy leaks across the SiN into the Si frame. Once the energy departs into the thermal bath, the detector is ready for the next alpha strike. The thermal time constant for the alpha detector is 10 ms, which is much faster than typical alpha counting rates.

Alpha particle pulses are measured by reading out the TES thermometer. The TES is heated from 80 mK to its transition of 140 mK by voltage biasing with a shunt resistor (R_{sh}) shown in Fig. 2. Voltage biasing the superconductor results in negative electrothermal feedback.[19] The absorption of an incoming alpha particle increases the temperature of the TES and thereby its resistance. The current across the TES will then drop to maintain constant voltage and reduce the Joule heating. By operating in this way, the TES response is faster, the resolution of the TES is improved, and the stability requirements on the cryostat temperature are reduced.[19] The change in current is amplified by inductively coupling to a single superconducting quantum interference device (SQUID) that is mounted on the 80 mK stage, and is labeled SQ1 in Fig. 2. The changing current output from SQ1 is then amplified by a 50 SQUID series array[20] (SQA) held at 4 K. The output current of the SQA is proportional to the alpha particle energy. Also, the output is used as feedback to linearize the response of SQ1. The feedback current is fed through a resistor chosen to maximize the use of bits in the digitizer and the resultant voltage is amplified at room temperature with a 3 kHz, 6 dB low pass filter. The output from the amplifier is digitized by a 14 bit analog-to-digital converter. The digitizer is run in triggered mode. However, in

Downloaded 07 Sep 2010 to 132.163.130.218. Redistribution subject to AIP license or copyright; see http://jap.aip.org/about/rights_and_permissions

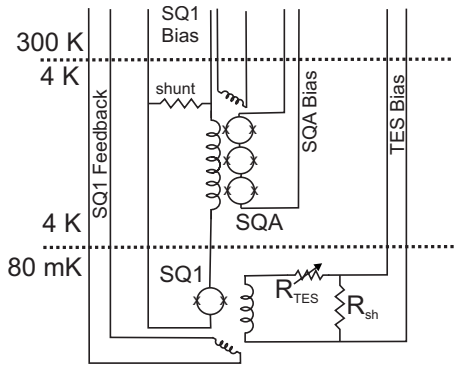

FIG. 2. The bias and amplification chain for the TES detector. The TES thermometer, R_{TES}, is shunted by an approximately 500 $\mu\Omega$ resistor, R_{sh}. All bias voltages are supplied by batteries that are unconnected to any external circuits. The current through the TES is amplified by a SQUID at 80 mK, labeled SQ1. The current from SQ1 is then amplified by an array of SQUIDs, labeled SQA. The output from SQA is used as the measured signal as well as the feedback to SQ1. Also shown in the circuit is the temperature where each component is maintained. The 80 mK stage is the ADR, while the 4 K stage is maintained by liquid helium, and 300 K is outside the cryostat.

order to measure noise traces, the digitizer is allowed to freely trigger and any traces that register pulses are removed before analyzing the noise.

The detector package is placed in vacuum where it is cooled and maintained at 80 mK using an adiabatic demagnetization refrigerator (ADR).[21] A heat sunk aluminum aperture is placed over the absorber as is shown schematically in Fig. 3. An aluminum shield is then attached to the detector stage which protects the detector from impinging 4 K radiation from the cryostat, also shown in Fig. 3. The temperature of the ADR stage is controlled by applying a magnetic field to the attached paramagnetic salt. The thermometer on the ADR stage is a ruthenium oxide resistor. A feedback loop is used to maintain the temperature by slowly reducing the current through the ADR magnet as the cryostat warms. The temperature of the stage must be below the transition temperature of the TES which is 140 mK. In practice, however, the temperature of the ADR stage affects the resolution of the detector so the lower the stage temperature, the better the detector performs. A temperature of 80 mK allows run times of up to 14 h.

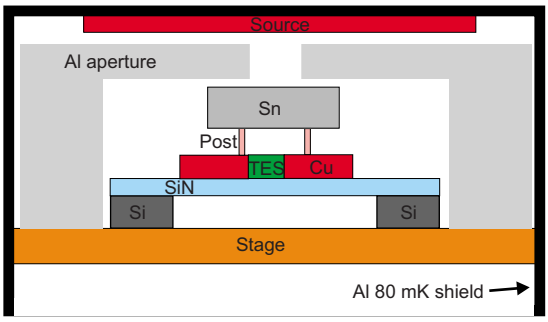

FIG. 3. (Color online) Schematic sideview (not to scale) of the alpha detector. The aperture is a single Al piece that screws to the stage and has a hole above the Sn absorber. The stage is made of gold-plated copper. Surrounding the whole stage is an Al shield, thermally sunk to the stage. The alpha emitter is spontaneously deposited on a Pt planchet that is glued to the inside of the shield above the detector.

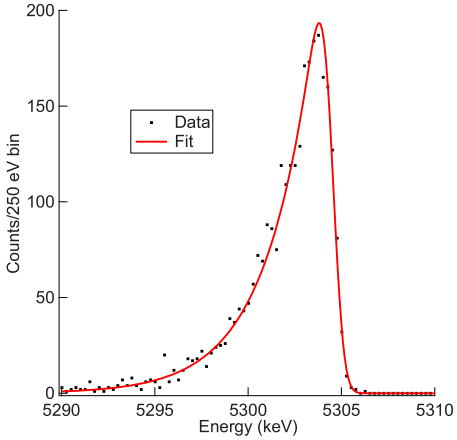

FIG. 4. (Color online) Microcalorimeter spectrum of ^{210}Po alpha emission.

The quality of the temperature regulation is improved by an appropriate choice of excitation current. The minimum excitation current of the resistance bridge, however, is 10 nA and the temperature was set to 80 mK with this excitation. The excitation was then increased to 30 nA and the self heating of the thermometer raised the readout temperature to 85 mK. Since the higher current excitation reduced the noise of the temperature readout, the temperature is set to 85 mK with the higher excitation and the temperature is understood to actually be 80 mK.

Both alpha particles and gamma-rays are used to characterize the detector. For alpha particles, the radioactive source is a platinum planchet with one side spontaneously deposited with the alpha emitters ^{210}Po and ^{209}Po. The planchet is glued to the inside of the 80 mK aluminum detector shield with the deposited side facing the detector, as is shown in Fig. 3. We also measure gamma-ray photons with 100 keV energy. The Sn absorber on the alpha microcalorimeter is 20% efficient for 100 keV photons. The gamma-ray source is ^{153}Gd which is placed outside the cryostat.

III. RESULTS AND DISCUSSION

A. Achieved resolution

Microcalorimeter behavior is characterized using alpha particles emitted by isotopes of Po. The isotope ^{210}Po is an ideal source because it easily deposits as a very thin layer and has a single alpha emission line at 5304.38 keV. An energy spectrum from ^{210}Po is shown in Fig. 4. The detector resolution determines the width of the high energy broadening at approximately 5305 keV. The low energy tail in the spectrum is termed straggling. Straggling occurs when alpha particles lose energy that is not collected in the detector. Straggling can come from several effects including energy loss in sources of finite thickness and, in semiconductor detectors, a surface dead layer on the detector itself. Microcalorimeters are not expected to have a surface dead layer since they measure energy rather than charge. The use of an aperture over the microcalorimeter also induces some straggling from alphas that scatter off the inner circumference before reaching the detector. However, simulations with Geant4 show that the great majority of alpha particles absorbed by

Downloaded 07 Sep 2010 to 132.163.130.218. Redistribution subject to AIP license or copyright; see http://jap.aip.org/about/rights_and_permissions

the detector are unaffected by the aperture so that the resolution is unchanged. Ion induced lattice damage is another candidate source of straggling and we predict the shape and magnitude of this effect in Sec. III D.

In order to extract quantitative values for the resolution and straggling, the spectrum in Fig. 4 is fitted with a convolution of a Gaussian detector response with a left-handed decaying exponential to model straggling. The resulting line shape is given by

$$f(x) = \frac{A}{2\tau}\mathrm{Exp}\left(\frac{x-x_0}{\tau} + \frac{\sigma^2}{2\tau^2}\right)\mathrm{Erfc}\left[\frac{1}{\sqrt{2}}\left(\frac{x-x_0}{\sigma} + \frac{\sigma}{\tau}\right)\right], \tag{1}$$

where A is the peak area, τ is the exponential decay of the straggling, x_0 is the peak location, and σ is the Gaussian width so that 2.355σ is the FWHM of the detector response.[22] The energy calibration is done assuming a locally linear response between the known peak energies from ^{210}Po (5304.38 keV) and the excited state alpha decay of ^{209}Po (4883 keV). The peak positions (in voltage) are determined from fitting ^{210}Po and ^{209}Po spectra using Eq. (1) to determine values of x_0. The initial detector which achieved 1.06 keV resolution[6] was broken after several experimental runs while being removed from the cryostat. The detector used to measure the spectrum in Fig. 4 is another chip from the same wafer. Fitting the calibrated spectrum in Fig. 4 yields a resolution of 1.09 ± 0.06 keV FWHM. The straggling parameter, τ, is 2.55 ± 0.06 keV. We next show that the resolution is significantly worse than the expected detector response.

B. Expected detector response

In microcalorimeters, power fluctuations across the thermal isolation limit the FWHM accuracy of the energy measurement. For a simple microcalorimeter, the resolution is given by,

$$\Delta E_{\mathrm{FWHM}} \approx 2.355\xi(kT^2C)^{1/2}, \tag{2}$$

where k is Boltzmann's constant, T is the microcalorimeter temperature, C is the heat capacity of the isolated body, and ξ is a dimensionless measure of the sensitivity of the thermometer.[23] Equation (2) shows that benefits in resolution follow directly from cooling to low temperatures. Assuming 5 MeV particles, realistic parameters $T=0.14$ K, $C=250$ pJ/K, and $\xi=1$ lead to a predicted energy resolution of 0.12 keV. In practice, the energy resolution expression must be modified to include thermal impedances within the sensor and the detailed properties of the superconducting transition.[8,24] Hence, Eq. (2) establishes the feasibility of resolution values near 0.1 keV but does not prove that we have obtained such a performance level.

The intrinsic resolution of a microcalorimeter can be experimentally determined by two techniques. First, we can measure the signal-to-noise ratio of alpha pulses. The average of 200 alpha pulses from ^{210}Po is shown in Fig. 5(a) and the frequency-domain spectral density of this average pulse is shown in Fig. 5(b). Also shown in Fig. 5(b) is the frequency-domain spectral density of the detector noise obtained by freely triggering the digitizer connected to the sensor, fourier-transforming each record, and averaging the transforms. The resolving power of the sensor after application of a so-called optimal filter is then given by

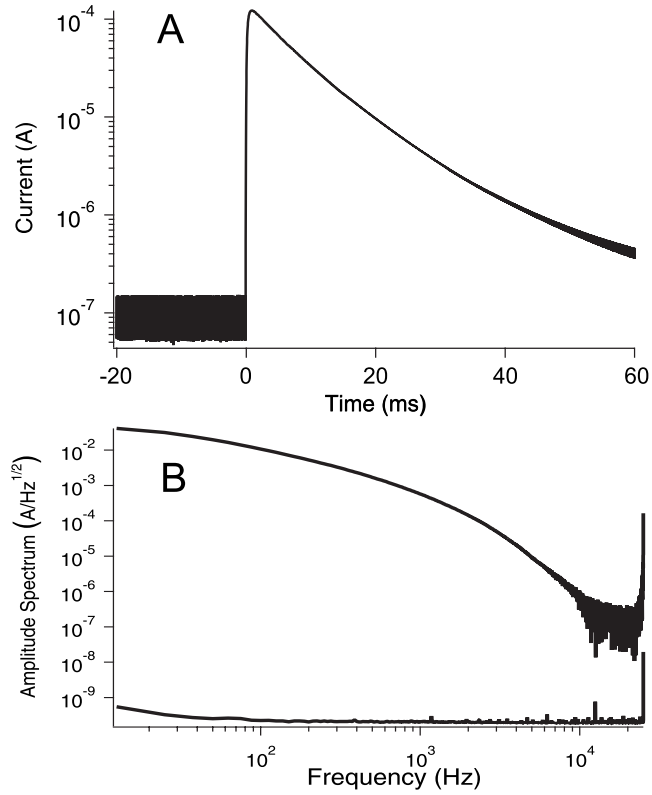

FIG. 5. (a) Average current pulse from ^{210}Po (log scale). Although the pulse shown is positive, physically it is a reduction in current through the TES. The baseline represents zero current reduction where an offset has been added to allow plotting on log scale. The initial pulse decay is exponential with a time constant of 10 ms. (b) The average pulse and average noise in the frequency domain.

$$\frac{F_{max}}{\Delta F_{rms}} = \frac{\int_{-\infty}^{\infty}\frac{S^2(f)}{N^2(f)}df}{\sqrt{\int_0^{\infty}|S(f)/N^2(f)|^2N^2(f)df}}, \tag{3}$$

where F_{max} is the signal maximum after filtering, F_{rms} is the filtered noise, $S(f)$ is the unfiltered signal in frequency space, and $N(f)$ is the unfiltered noise in frequency space.[25] Using Eq. (3), and the average pulse and noise in Fig. 5(b), the predicted resolving power is 14 063 which corresponds to a resolution of 0.380 keV at 5.3 MeV, provided the detector response is linear.

The second determination of the thermodynamic sensor resolution is to measure lower energy events and to extrapolate performance at 5.3 MeV. As can be seen from Eq. (2), microcalorimeter resolution is independent of the incoming energy, provided the detector response is linear. As shown in Fig. 6, we measured the spectrum from a ^{153}Gd source which provides two prominent peaks at 97.431 and 103.18 keV. The two peaks provide a reliable local energy calibration. The resolution prediction for the Gd photons is 104.6 eV FWHM and the achieved resolution is 102.1 ± 0.4 eV, which is very close to the prediction of Eq. (2). The discrepancy between

Downloaded 07 Sep 2010 to 132.163.130.218. Redistribution subject to AIP license or copyright; see http://jap.aip.org/about/rights_and_permissions

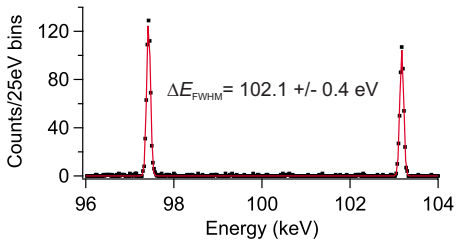

FIG. 6. (Color online) Spectrum from a ^{153}Gd source. The detector resolution is 102.1 eV.

the photon resolution and that predicted from the alpha pulses is due to additional noise contributed to the alpha spectrum at lower amplifier gain. This will be discussed further. It is apparent from this result, however, that the thermodynamic resolution of the alpha detector can be achieved by photons. Thus, there is a mechanism for resolution degradation that is specific to the measurement of particles.

The discrepancy between the measured gamma-ray resolution and the predicted alpha particle resolution is due to additional noise from the room temperature amplifier chain. The reason is that the 50× lower gain used for alpha spectra allowed either the output noise of the room temperature amplifier or the input noise of the digitizer to dominate the total noise. In order to verify this explanation, the noise recorded from the gamma-ray measurement was divided by 50 to mimic the gain settings for an alpha acquisition and the signal-to-noise was calculated from Eq. (3) utilizing this modified gamma-ray noise and the alpha pulses. The result is a predicted resolution of 103.6 eV FWHM. While the additional room temperature noise has very little effect on the achieved 1.09 keV alpha resolution, if the thermodynamic resolution for the alpha particle detector is reached, it will be a significant noise source to address. The key conclusion is that the absolute thermodynamic resolution limit of the alpha particle microcalorimeter is approximately 100 eV. There is an additional 365 eV electronic noise in the current configuration in order to have sufficient dynamic range for alpha acquisition.

Both measurements of the thermodynamic resolution are contingent on the linearity of the sensor. A plot of all the energies measured is shown in Fig. 7. Unfortunately, alpha particles are only emitted in the 4–6 MeV range and we do not have access to photons over 104 keV. To assess linearity, we fit a line to the two gamma-ray peaks and the origin. The slope of this line is compared to the slope defined by the two alpha particle peaks alone. The slope for the gamma-ray photons is 6705 ± 2 keV/V, while the slope for the alpha particles is 6446 ± 4 keV/V. The slope difference reveals only a 4% deviation from linearity at 5 MeV. The alpha detector has a slightly increased response at the higher energies. Thus, the thermodynamic resolution at 5.3 MeV determined from lower-energy gamma-rays is 98.0 eV. In what follows, we review and reject possible causes for the discrepancy between the 0.1/0.3 keV thermodynamic/electronic resolution and the measured 1.09 keV alpha particle resolution.

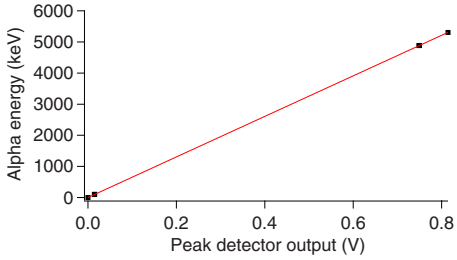

FIG. 7. (Color online) Plot of known gamma-ray photon and alpha particle energies vs their measured voltage. The line is a linear fit to all the points.

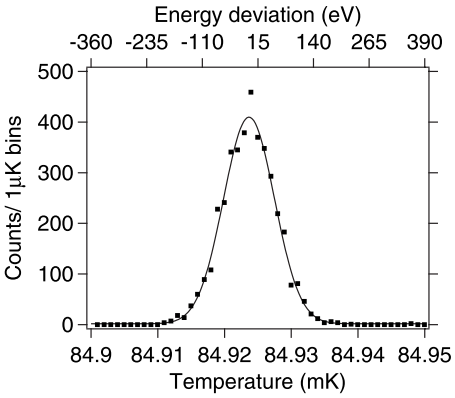

FIG. 8. Fluctuations in cryostat temperature and corresponding energy fluctuations during spectrum acquisition. Each count corresponds to a 10 s interval.

C. Mechanisms of resolution degradation

One mechanism that can cause a discrepancy between the resolution predicted from signal-to-noise measurements and the achieved resolution is position dependence in the Sn absorber. If the time for heat to diffuse from the absorber into the TES thermometer depends on the absorption position, then the output pulses of the TES will depend on the absorption position and even a noiseless detector responding to monoenergetic alpha particles will show a broadened response. In order to look for position dependence, we acquired spectra with a range of aluminum apertures between the detector and source so as to restrict the region of the absorber illuminated with alpha particles. With an aperture of 3 mm diameter and an absorber of area of 4×4 mm^2, we achieved a resolution of 2.4 keV FWHM for a ^{210}Po source. By reducing the size of the absorber to 1.7×1.7 mm^2 and the aperture diameter to 1.4 mm we improved the resolution to 1.34 keV FWHM. Next, we changed only the aperture diameter from 1.4 to 0.7 mm in diameter. This change improved the resolution to 1.06 keV, clearly indicating the presence of position dependence. We then reduced the aperture diameter to 0.35 mm, but observed no further improvement in resolution. Hence, the final resolution figure of 1.06 keV does not include a contribution from position dependence and all data used in this study utilize the 0.35 mm aperture.

We also investigated the effect of cryostat temperature fluctuations on sensor resolution. First, we recorded a spectrum from ^{210}Po where the set point of the cryostat temperature was 84.9 mK. During the 11 h acquisition, the cryostat temperature was recorded every 10 s and the resulting distribution of temperatures is shown in Fig. 8. Next, the set point was changed to 85 mK and the shift in the position of the

Downloaded 07 Sep 2010 to 132.163.130.218. Redistribution subject to AIP license or copyright; see http://jap.aip.org/about/rights_and_permissions

^{210}Po peak was used to determine an energy dependence on temperature of 0.015 keV/μK. Hence, the 8.95 μK FWHM temperature distribution in Fig. 8 corresponds to an energy broadening of 134 eV FWHM.

The next resolution degradation mechanism that we consider is the sputtering of atoms from the absorber by incident alpha particles. Kinetic energy used to eject atoms from the absorber is lost to our thermometer and fluctuations in this energy will be an additional noise source. We investigated sputtering losses using the Monte Carlo code SRIM.[26] This code uses the Kinchin–Pease model to follow the cascades of atoms set in motion by alpha particles. The cascade statistics depend on three parameters of the absorber lattice: the displacement energy, E_D, lattice binding energy, E_L, and surface binding energy, E_B. For sputtering, the most important energy is E_B which is the energy barrier to removing an atom from the surface of the material into vacuum. The displacement energy E_D is the energy barrier to moving an atom in the absorber from its lattice site, and the lattice binding energy E_L is the energy lost by an atom removed from a lattice site. We run the SRIM code for 5304.38 keV He ions normally incident on 250 μm thick Sn. We assume a displacement energy of 28 eV,[27] a surface binding energy of 3.12 eV,[26] and a lattice binding energy of 3 eV.[28] The SRIM calculation predicts a typical penetration depth of 16 μm and that no atoms are sputtered. For 5.3 MeV alpha particles, most energy loss is to ionization so that the alpha particle must slow considerably before nuclear collisions which lead to atomic movement play a role.[29] Thus, the penetration is deep enough and the resulting cascades short enough that sputtering does not occur.

A related energy degradation mechanism is the ejection of secondary electrons from the surface of the absorber. To assess this possibility, we use the expression of Schou[30] for the number of electrons emitted as a function of emission energy. By multiplying and integrating over energy, we obtain the expression for total emitted energy

$$E_e = \int_{U_0}^{\infty} \frac{\Gamma_m D(x=0,E,\vec{e})(E_1 - U_0)^2(1-m)dE_1}{4N_C E_1^{1-2m} E_1^2}. \quad (4)$$

The function, Γ_m, is defined by Schou[30] as

$$\Gamma_m = \frac{m}{\psi(1) - \psi(1-m)}, \quad (5)$$

where,

$$\psi(x) = \frac{d}{dx}\ln \Gamma(x). \quad (6)$$

$\Gamma(x)$ is the gamma function and m=−2.5. Here, U_0 is the binding energy of electrons at the surface which is the sum of the work function and the fermi energy of the absorber metal. For Sn, U_0 is 14.6 eV. The term D is the instantaneous energy given by the incoming alpha particle to ionization in the absorber at the surface, $x=0$, for incoming alpha energy E and angle, $\vec{e}$. This term is taken from SRIM to be approximately 25 eV. The term $N_C E_1^{1-2m}/(1-m)$ is a power law approximation to the electron stopping power in the absorber and N_C is estimated to be 2.75×10^{-9} eV^{2m}/Å.[30] Finally, E_1 is the energy of the emitted electron. This integration yields a total electron energy loss from Sn of 330 eV. Dividing the integrand by energy E_1 and repeating the integral yields an average of 17 electrons emitted per ion. Taking the average energy of each electron to be 19.4 eV, normal fluctuations in the number of electrons emitted will yield an energy fluctuation of 80 eV. Thus, secondary electron emission is predicted to be a minor contributor to resolution degradation.

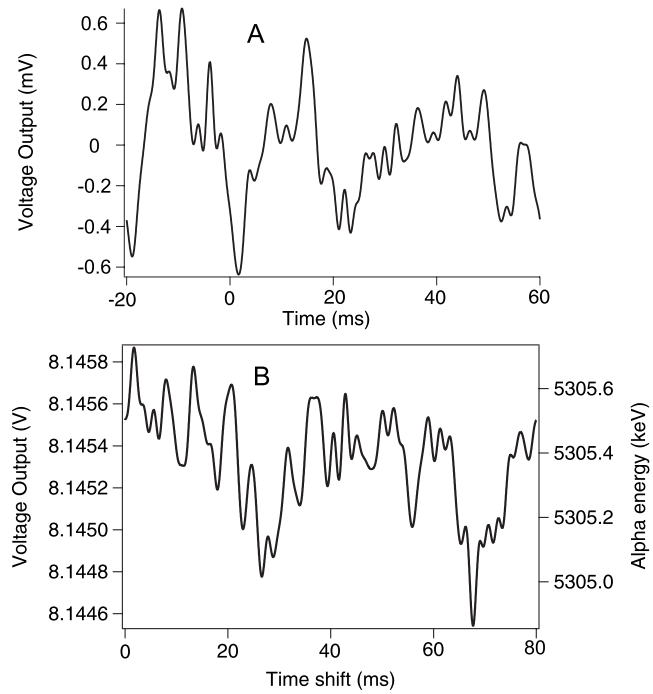

FIG. 9. (a) An optimally filtered noise trace taken just before the spectrum shown in Fig. 4. The average value has been offset to 0 V. (b) Plot of pulse height from ^{210}Po vs time shift in noise record. A histogram of the plotted alpha energies has a FWHM of 340 eV.

Measurements in the literature for similar, but not identical, conditions confirm that secondary electron emission can be ignored. For example, Svensson[31] measured an electron yield of less than three electrons for 350 keV helium ions incident on aluminum with the yield saturating for higher energies. Koyama[32] measured the electron yield of 5 MeV alpha particles incident on nickel and also found three electrons per ion emitted. Hence, our calculation for Sn may represents an upper bound on this noise source.

Another possible mechanism that we consider is the contribution of the relative phase between noise and pulses. The optimal filter technique described in Sec. III B ignores the phase of the noise. Hence, the effect of noise tones at frequencies near the characteristic timescale of the pulses may be worse than predicted by Eq. (3). As an example, the 16 ms period of line power is dangerously near the 10 ms decay time of the pulses. To assess this effect, we optimally filtered noise records taken before the data of Fig. 4. One such filtered noise record is shown in Fig. 9(a). The filtered noise record is then added to the filtered average pulse from ^{210}Po and the peak height is recorded. This process is repeated N times where N is the number of samples in a pulse record with the filtered noise record cyclically shifted in time by M samples where M ranges from 1 to N before it is added to the

Downloaded 07 Sep 2010 to 132.163.130.218. Redistribution subject to AIP license or copyright; see http://jap.aip.org/about/rights_and_permissions

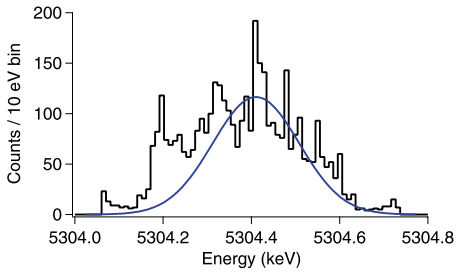

FIG. 10. (Color online) Histogram of pulse height variation shown in Fig. 9.

filtered average pulse. This measurement should yield the predicted signal-to-noise resolution and any resolution degradation from phase dependent noise. Deduced peak heights are plotted versus time shift in Fig. 9(b). A histogram of the energy fluctuation is shown in Fig. 10 as well as a Gaussian fit to the data. This calculation was performed on 10 noise traces and an average fluctuation of 340 ± 80 eV FWHM is found. Since this is approximately the resolution found from Eq. (3), phase dependent noise plays no role in the the broadening of the detector resolution.

Since we are sensitive to pulse height changes as small as a part in 10^4, we also look at whether corrections for gain drift are done accurately. This is equivalent to phase noise at frequencies corresponding to intervals much longer than the record length. The data shown in Fig. 4 have had a second order polynomial subtracted from the filtered pulse heights to account for temporal variations over the 13 h acquisition period. As a check of this procedure, polynomial corrections up to seventh order were also applied with no difference in the resulting resolution from the second order correction. Thus, gain drift is not playing a role in the resolution of the alpha detector.

There is also a possibility that the material properties of the superconducting absorber are causing some resolution broadening. Historically, superconducting absorbers on microcalorimeters have shown unexplained, long decays.[33] These anomalous decays may be due to additional degrees of freedom, such as quasiparticles, that affect the thermalization of energy deposited by photons or particles, thus providing a mechanism for fluctuations. An upper limit on these fluctuations can be derived from data using Sn absorbers by Bacrania *et al.*[34] on gamma-ray microcalorimeters. One microcalorimeter in an array achieved a resolution of 21.5 eV FWHM for a 103.18 keV gamma ray. The predicted resolution was 20.6 eV. The missing fluctuation energy, scaled from 100 to 5300 keV yields 320 eV in fluctuations that may be due to anomalous thermalization physics in the superconducting absorber.

D. Lattice damage

Previously, we rejected or quantified all known noise sources that could cause a discrepancy between the intrinsic and achieved sensor resolution. Subtracting contributions of 380 eV FWHM due to thermodynamic and room temperature amplifier noise, 134 eV FWHM due to temperature fluctuations, 80 eV due to electron ejection, and 320 eV due to possible thermalization effects in the absorber from the achieved resolution of 1.09 keV reveals a previously unrecognized noise term of 960 eV FWHM. These results are summarized in Table I. We observed a similar noise term in two additional devices from the same Si wafer measured in our laboratory, two devices from the same Si wafer measured in a second cryostat in a second laboratory, and two devices where the thin-film circuitry was fabricated in a different laboratory and the measurements were conducted in the second cryostat. Hence, a new noise limit has been encountered.

TABLE I. Resolution degradation mechanisms.

Mechanism	Energy fluctuation (eV)
Total measured resolution	1090
Thermodynamic	98
Room temperature amplification	365
Temperature fluctuations	134
Electron emission	80
Anomalous thermalization	320
Total degradation in quadrature	520
Unaccounted energy fluctuation	960

We next consider lattice damage as the origin of this new noise limit. Kinetic energy from the initial alpha particle that is converted to potential energy in the lattice of the absorber is lost to our thermometer and fluctuations in this energy are a noise source. The potential energy of the lattice is increased when its atoms are displaced to interstitial sites by collisions with an alpha particle or with other lattice atoms set in motion by an alpha particle. The combination of a vacant lattice site and an interstitial atom is called a Frenkel pair.

The dynamics of Frenkel pair production are governed by the energies shown in Fig. 11.[35] For an atom in the Sn lattice to be set in motion, it must be given enough energy to overcome the displacement energy, E_D. The atom will lose energy to ionization and further atomic collisions until it stops in an interstitial site or fills a vacancy. Most displaced atoms come to rest in interstitial sites, thereby increasing the potential energy of the lattice by an amount $E_F = E_L + E_I$ termed the Frenkel storage energy.

Because of the uncertainty in the materials parameters for Sn, and because the lack of detail in Andersen's work prevents our repeating his calculation explicitly for Sn, we

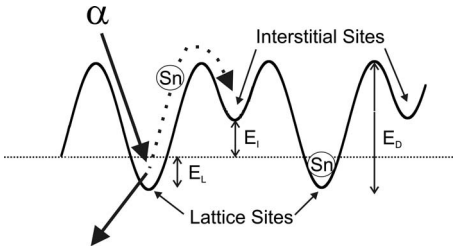

FIG. 11. Schematic potential energy curve. Two lattice sites are shown with energy E_L relative to the vacuum energy. The energy barrier to leave a lattice site is E_D and the energy cost for atoms that come to rest at an interstitial site is E_I. The potential energy of a Frenkel pair, a vacancy and an interstitial, is $E_F = E_L + E_I$. The formation of a Frenkel pair by an incoming alpha particle is shown schematically, although the vacancy-interstitial pairs are also formed by cascading Sn atoms.

Downloaded 07 Sep 2010 to 132.163.130.218. Redistribution subject to AIP license or copyright; see http://jap.aip.org/about/rights_and_permissions

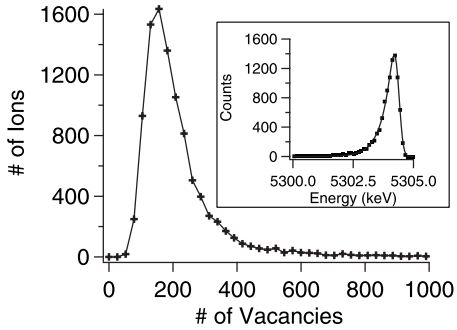

FIG. 12. (Main) Plot of ions vs number of vacancies created in Sn absorber. (Inset) Also shown is a plot of the resulting alpha particle spectrum assuming monoenergetic particles emitted from a ^{210}Po source. The spectrum shown assumes a displacement energy of 28 eV, lattice energy of 3.14 eV, and surface binding energy of 3 eV. The spectrum yields a resolution of 0.3 keV FWHM.

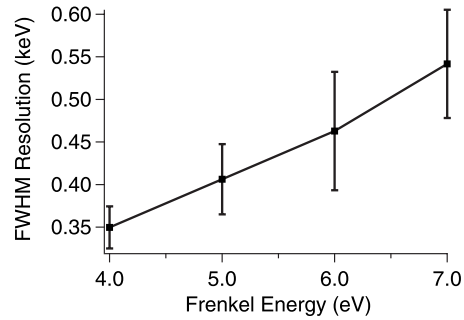

FIG. 13. Plot of expected microcalorimeter resolution from lattice damage vs Frenkel energy. The error bars correspond to the spread in published displacement energies.

used the code SRIM to compute the fluctuations in the number of Frenkel pairs. SRIM follows each alpha particle through the absorber and computes the number of Frenkel pairs the particle creates. The code neglects channeling effects and anisotropy of the displacement energy, which are reasonable to ignore for the polycrystalline material studied here. Also, SRIM does not account for any annealing of point defects due to localized heating by impinging alpha particles. By running the code iteratively and histogramming the results as shown in Fig. 12, we can determine the distribution of damage events. The energy measured by our sensor is the energy of the incident alpha particle minus the number of Frenkel pairs multiplied by E_F. It can be seen from the inset to Fig. 12 that predicted alpha spectra which include only Frenkel pair creation as a noise source have both a broadened high energy shoulder and an exponential low energy tail.

Andersen[16] is unique in having calculated the fluctuations in the number of Frenkel pairs created by incident alpha particles. Andersen[16] used estimates by Whitehead and Haines[29] for the energy given to atomic movement by the alpha particle to arrive at a resolution degradation figure of 1 keV for a Cu absorber. The displacement energy and Frenkel storage energy for Cu are 30 and 4.6 eV, respectively.[27] The equivalent numbers for a Sn absorber are similar in magnitude but less well known. The displacement energy in Sn ranges from 22–28 eV depending on the crystal orientation.[27] The lattice binding energy is 3.14 eV.[28] The Frenkel pair energy is not known, but is often about twice the binding energy suggesting a value of 4–6 eV. Hence, Andersen's calculation of 1 keV for Cu may also be applicable to Sn; certainly, it is very close to our measured noise value of 0.95 keV.

There is a significant quantitative discrepancy between the predictions of Andersen and those of SRIM for the fluctuations in the energy lost to lattice damage. This discrepancy is not caused by the uncertainties in the lattice parameters of Sn. The resolution broadening predicted by SRIM is plotted in Fig. 13 as a function of Frenkel pair energy for the extremes of displacement energy. The maximum predicted broadening is 0.65 keV, considerably smaller than the predictions of Andersen and our measurements. Hence, SRIM's treatment of vacancy production may not be quantitatively accurate. Figure 13 also highlights an important future capability of microcalorimeter alpha spectrometry. The error bar on a microcalorimeter determination of the lattice damage noise is estimated to be only 100 eV, which, as shown in Fig. 13 will allow the lattice parameters to be tightly constrained once there is an agreed-upon theoretical framework. Hence, microcalorimeter alpha spectrometry can be used both to evaluate atomic cascade theories and to determine lattice parameters in previously unstudied materials.

As mentioned previously, microcalorimeters are expected to show less straggling than sensors that rely on charge collection because microcalorimeters do not have a surface dead layer. However, the low energy tail on the inset to Fig. 12 demonstrates that Frenkel pair creation is a source of straggling in microcalorimeters (and other types of sensors as well). The straggle parameter for the spectrum of Fig. 12 is 0.456 ± 0.006 keV which increases to 1.46 keV when multiplied by the same factor needed to make the Frenkel noise match the achieved resolution. In contrast, the straggle parameter in the measured ^{210}Po spectrum of Fig. 4 is 2.55 keV. Understanding and minimizing straggle is important for analytical alpha spectrometry applications where the achieved resolution of 1.06 keV is already much smaller than the line separations of interest (for instance, the strongest emissions from 239 Pu and 240 Pu are separated by 11.6 keV). For these applications, reducing the straggle parameter will produce far greater spectral clarity than further resolution improvements.[6] In addition, understanding the relative magnitudes of straggle from the instrument and straggle from the source is required in order to know how much effort should be invested in developing chemical preparation techniques that produce cleaner, thinner, and more homogeneous layers of source material.[36]

IV. CONCLUSION

The microcalorimeter alpha particle detector has achieved a FWHM resolution as good as 1.06 ± 0.06 keV for 5.3 MeV alpha particles. This resolution is the highest resolving power for any energy dispersive technique and is sufficient for the detector to be put to use in various analytical applications. However, the intrinsic resolution of the detector is 0.1 keV. We have assessed numerous potential sources of peak broadening and conclude that most of the discrepancy between the intrinsic and achieved resolutions,

Downloaded 07 Sep 2010 to 132.163.130.218. Redistribution subject to AIP license or copyright; see http://jap.aip.org/about/rights_and_permissions

0.96 keV, is due to fluctuations in the lattice damage caused by the absorbed ions. The unique ability of the microcalorimeter to determine the variation in atomic cascades created by monoenergetic alpha particles is a new tool to test theories of cascade dynamics. For instance, we have shown that the predictions of the ubiquitous code SRIM for the Frenkel noise are a factor of 2 smaller than measurements. In the future, microcalorimeter data may allow more accurate measurements of lattice parameters such as the displacement and Frenkel pair energies.

ACKNOWLEDGMENTS

We acknowledge valuable technical discussions with Harvey Moseley, Galen O'Neil, and Minesh Bacrania. We gratefully acknowledge the support of the U.S. Department of Energy through the Office of Nonproliferation Research and Development, the LANL/LDRD Program, and the Department of Homeland Security for this work. RDH acknowledges support through NSF (under Grant No. IIS 0813777).

[1]P. L. Kapitza, Proc. R. Soc. London, Ser. A **48**, 102 (1924).
[2]P. Sigmund, *Particle Penetration and Radiation Effects* (Springer-Verlag, Berlin, 2006).
[3]S. A. Campbell, *The Science and Engineering of Microelectronic Fabrication* (Oxford University Press, New York, 1996).
[4]K. J. Moody, I. D. Hutcheon, and P. M. Grant, *Nuclear Forensic Analysis* (CRC Press, Boca Raton, 2005).
[5]E. Steinbauer, P. Bauer, M. Geretschlager, G. Bortels, J. P. Biersack, and P. Burger, Nucl. Instrum. Methods Phys. Res. B **85**, 642 (1994).
[6]R. D. Horansky, J. N. Ullom, J. A. Beall, G. C. Hilton, K. D. Irwin, D. E. Dry, E. P. Hastings, S. P. Lamont, C. R. Rudy, and M. W. Rabin, Appl. Phys. Lett. **93**, 123504 (2008).
[7]B. Cabrera, R. Clarke, A. Miller, S. Nam, R. Romani, T. Saab, and B. Young, Physica B **280**, 509 (2000).
[8]J. N. Ullom, J. A. Beall, W. B. Doriese, W. D. Duncan, L. Ferreira, G. C. Hilton, K. D. Irwin, C. D. Reintsema, and L. R. Vale, Appl. Phys. Lett. **87**, 194103 (2005).
[9]B. L. Zink, J. N. Ullom, J. A. Beall, K. D. Irwin, W. B. Doriese, W. D. Duncan, L. Ferreira, G. C. Hilton, R. D. Horansky, C. D. Reintsema, and L. R. Vale, Appl. Phys. Lett. **89**, 124101 (2006).
[10]W. Doriese, J. Ullom, J. Beall, W. Duncan, L. Ferriera, G. Hilton, R. Horansky, K. Irwin, J. Mates, C. Reintsema, L. R. Vale, Y. Xu, B. L. Zink, M. W. Rabin, A. S. Hoover, C. R. Rudy, and D. T. Vo, Appl. Phys. Lett. **90**, 193508 (2007).
[11]G. C. Hilton, J. M. Martinis, D. A. Wollman, K. D. Irwin, L. L. Dulcie, D. Gerber, P. M. Gillevet, and D. Twerenbold, Nature (London) **391**, 672 (1998).
[12]S. Niemeyer and L. Koch, "The Nuclear Smuggling International Technical Working Group: Making a Difference in Combating Illicit Trafficking, IAEA-CN-98/3," p. 17, in Advances in Destructive and Non-Destructive Analysis for Environmental monitoring and nuclear forensics, Proceedings of International Conference, Karlsruhe, 21–23 October 2002 (IAEA, Vienna, 2003).
[13]Report of the Joint Working Group of the American Physical Society and the American Association for the Advancement of Science, Nuclear Forensics Role State of the Art, Program Needs, 2008.
[14]Royal Society Policy Statements 2008.
[15]M. P. Croce, M. K. Bacrania, A. S. Hoover, M. W. Rabin, N. J. Hoteling, S. P. LaMont, A. A. Plionis, D. E. Dry, J. N. Ullom, D. A. Bennett, R. D. Horansky, V. Kotsubo, and R. Cantor, AIP Conf. Proc. 1185, 741 (2009).
[16]H. H. Andersen, Nucl. Instrum. Methods Phys. Res. B **15**, 722 (1986).
[17]A. Juillard, Ph.D. thesis, Universite de Paris, 1999.
[18]K. D. Irwin and G. C. Hilton, *Cryogenic Particle Detection*, Topics Appl. Phys. Vol. 99 (Springer-Verlag, Berlin, 2005), pp. 63–149.
[19]K. D. Irwin, Appl. Phys. Lett. **66**, 1998 (1995).
[20]R. P. Welty and J. M. Martinis, IEEE Trans. Magn. **27**, 2924 (1991).
[21]C. Hagmann and P. Richards, Cryogenics **34**, 221 (1994).
[22]G. Bortels and P. Collaers, Appl. Radiat. Isot. **38**, 831 (1987).
[23]S. H. Moseley, J. C. Mather, and D. McCammon, J. Appl. Phys. **56**, 1257 (1984).
[24]M. Galeazzi and D. McCammon, J. Appl. Phys. **93**, 4856 (2003).
[25]K. D. Irwin, Ph.D. thesis, Stanford University, 1995.
[26]J. Ziegler, J. Biersaki, and U. Littmark, *The Stopping and Ranges of Ions in Solids* (Pergamon, New York, 1985).
[27]C. Broeders and A. Konobeyev, J. Nucl. Mater. **328**, 197 (2004).
[28]C. Kittel, *Introduction to Solid State Physics* (Wiley, New York, 1996).
[29]E. L. Haines and A. B. Whitehead, Rev. Sci. Instrum. **37**, 190 (1966).
[30]J. Schou, Phys. Rev. B **22**, 2141 (1980).
[31]B. Svensson and G. Holmen, J. Appl. Phys. **52**, 6928 (1981).
[32]A. Koyama, E. Yagi, and H. Sakairi, Jpn. J. Appl. Phys., Part 1 **15**, 1811 (1976).
[33]M. L. van den Berg, D. T. Chow, A. Loshak, M. F. Cunningham, T. W. B, Jr., M. Frank, and S. E. Labov, Proc. SPIE **4140**, 436 (2000).
[34]M. Bacrania, A. S. Hoover, P. J. Karpius, M. W. Rabin, C. R. Rudy, D. T. Vo, J. A. Beall, D. A. Bennet, W. B. Doriese, and G. C. Hilton, IEEE Trans. Nucl. Sci. **56**, 2299 (2009).
[35]K. Nordlund and R. S. Averback, J. Nucl. Mater. **276**, 194 (2000).
[36]A. A. Plionis, J. H. Rim, E. P. Hastings, S. P. LaMont, D. E. Dry, M. K. Bacrania, R. D. Horansky, J. N. Ullom, J. A. Beall, and M. W. Rabin, J. Radioanal. Nucl. Chem. **282**, 905 (2009).

Downloaded 07 Sep 2010 to 132.163.130.218. Redistribution subject to AIP license or copyright; see http://jap.aip.org/about/rights_and_permissions